Journal of Solid State Chemistry 183 (2010) 1998–2003

Contents lists available at ScienceDirect

Journal of Solid State Chemistry

journal homepage: www.elsevier.com/locate/jssc

Temperature and composition dependent structural investigation of the defect perovskite series $Sr_{1-x}Ti_{1-2x}Nb_{2x}O_3$, $0 \le x \le 0.2$

William R. Brant [a], Siegbert Schmid [a,*], Qinfen Gu [b], Ray L. Withers [c], James Hester [d], Maxim Avdeev [d]

[a] School of Chemistry, The University of Sydney, Sydney, NSW 2006, Australia
[b] Australian Synchrotron, 800 Blackburn Rd, Clayton, VIC 3168, Australia
[c] Research School of Chemistry, Australian National University, Canberra, ACT 0200, Australia
[d] Bragg Institute, Australian Nuclear Science and Technology Organisation, Menai, NSW 2234, Australia

ARTICLE INFO

Article history:
Received 1 April 2010
Received in revised form
27 May 2010
Accepted 4 June 2010
Available online 7 July 2010

Keywords:
Defect perovskite
Phase transition
Solid solution
Thermal expansion

ABSTRACT

The crystal structure of the defect perovskite series $Sr_{1-x}Ti_{1-2x}Nb_{2x}O_3$ has been investigated over a range of temperatures using high-resolution synchrotron X-ray diffraction, neutron diffraction and electron diffraction. Three distinct regions were observed: $0 < x \le 0.125$ was a solid solution of $Sr_{1-x}Ti_{1-2x}Nb_{2x}O_3$ with minor $SrTiO_3$ intergrowth, $0.125 < x \le 0.2$ was a pure $Sr_{1-x}Ti_{1-2x}Nb_{2x}O_3$ solid solution adopting the cubic perovskite type structure ($Pm\bar{3}m$) and for $x > 0.2$ $Sr_{0.8}Ti_{0.6}Nb_{0.4}O_3$ and $Sr_3TiNb_4O_{15}$ formed a two phase region. The cubic structure for $Sr_{0.8}Ti_{0.6}Nb_{0.4}O_3$ was stable over the temperature range 90–1248 K and the thermal expansion co-efficient was determined to be $8.72(9) \times 10^{-6}\,K^{-1}$. Electron diffraction studies revealed diffuse scattering due to local scale Ti/Nb displacements and slightly enhanced octahedral rotations that did not lead to long range order. The octahedral rotations were observed to 'lock-in' at temperatures below ~75 K resulting in a tetragonal structure ($I4/mcm$) with anti-phase octahedral tilting about the c-axis.

1. Introduction

Perovskite oxides are a class of materials represented by the formula ABO_3, whereby large A-site cations fill the voids created by the three dimensional network of corner linked BO_6 octahedra. Compositional flexibility induced through structural flexibility allows for a wide variety of cation combinations, which crystallise as a stable perovskite structure. The ideal aristotype cubic perovskite, however, does not form so frequently due to strict bonding requirements [1]. As a result most perovskites form distorted structures with BO_6 octahedral distortions or rotations being the most common form of structural alteration [2]. The changes introduced into the structure by octahedral distortions can be subtle and are often very hard to detect and characterise. In addition, the ion transport properties of defect perovskites can be altered significantly by structural changes on removal or addition of small atoms [3,4]. Thus precise structural determination of defect perovskites developed for applications, e.g. as anodes in solid oxide fuel cells or as a solid state electrolyte in lithium ion batteries, is essential.

$Sr_{1-x}Ti_{1-2x}Nb_{2x}O_3$ (STN), a defect perovskite series, has attracted a significant amount of research into its oxygen conduction properties and yet no high resolution diffraction studies have been conducted to investigate its structural behaviour. There have been conflicting reports in the literature about the extent of the STN solid solution as well as the symmetry adopted by the perovskite type structure. Initially, Tien and Moratis [5] reported that STN formed from $SrTiO_3$ up to a composition $Sr_{0.85}Ti_{0.7}Nb_{0.3}O_3$ ($x=0.15$) and that it formed a tetragonally distorted perovskite type structure. Irvine et al. [6] then established that the compound formed as a single phase up to a composition of $Sr_{0.8}Ti_{0.6}Nb_{0.4}O_3$ ($x=0.20$) with the cubic perovskite type structure. More recently, Kolodiazhnyi and Petric [7] reported that the series only formed a cubic perovskite up to a composition $Sr_{0.85}Ti_{0.7}Nb_{0.3}O_3$. While the vast majority of perovskite type structures deviate from the cubic symmetry at ambient conditions, the STN series may well form a cubic structure in analogy to $SrTiO_3$ and Sr_xNbO_3. The Sr_xNbO_3 solid solution has been reported to form a cubic perovskite structure in the range $0.7 \le x \le 0.95$ [8]. In order to maintain an overall neutral charge niobium adopts both the Nb(IV) and Nb(V) valence states. If Nb(IV) is replaced with Ti(IV) then the STN series is generated. Since the bond length of Nb^{5+} (1.965 Å) and Ti^{4+} (1.978 Å) to oxygen, as determined via bond valence sums [9], are roughly equivalent in an ideal undistorted octahedron it is reasonable to expect that STN too adopts a cubic structure. However, intermediate compositions with a high concentration of vacancies may exhibit increased structural flexibility around the vacant sites. It is

* Corresponding author.
E-mail address: siegbert.schmid@sydney.edu.au (S. Schmid).

0022-4596/$ - see front matter © 2010 Elsevier Inc. All rights reserved.
doi:10.1016/j.jssc.2010.06.002

possible that the structural flexibility will manifest as local structural distortions. Whether this distortion periodically translates through the structure leading to lower symmetries as observed by Tien and Moratis [5], or if it remains localised will be investigated.

In order to fully understand changes that occur in the structure in response to, e.g., oxygen conduction or Li ion intercalation it is vital that detailed high resolution diffraction studies are conducted of the parent material. Thus, the current study has two objectives. The first is to establish the compositional range over which STN forms as a pure phase with the aim to synthesise the species with the highest vacancy concentration for property evaluations. The second objective is to examine fine structural detail of high vacancy STN compositions over a range of temperatures. Therefore, in addition to ambient temperature studies via synchrotron X-ray diffraction, neutron diffraction and electron diffraction, low temperature studies using high resolution synchrotron X-ray and neutron diffraction were performed.

2. Experimental

Polycrystalline samples of several members of the $Sr_{1-x}Ti_{1-2x}Nb_{2x}O_3$ ($0 \le x \le 0.6$) series were prepared via conventional solid state reactions. Stoichiometric amounts of the starting materials $SrCO_3$ (Aldrich, 99.9+%), TiO_2 (Aithaca, 99.995%) and Nb_2O_5 (Aithaca, 99.998%) were finely ground in acetone using a mortar and pestle. The powder samples were heated at 1100 °C for 15 h then pressed into pellets and fired at 1300 °C for a further 24, 48 and 72 h with intermittent re-grinding. The powdered product was then heated at 500 °C for 20 h. The reaction progress was monitored using a PANalytical X'Pert PRO MPD X-ray diffractometer. Subsequent synchrotron X-ray, neutron and electron diffraction analyses were carried out on samples in the range $0 \le x \le 0.2$.

High resolution synchrotron X-ray powder diffraction (XRPD) patterns were collected over a wide range of temperatures on the powder diffraction beamline, 10-BM, at the Australian Synchrotron using the MYTHEN microstrip detector [10] and a Si(111) monochromator. Using LaB_6 (NIST standard 660a) the wavelength was accurately refined. Samples for collection at room temperature and low temperature were packed into 0.3 mm glass capillaries. Samples for collection at high temperature were packed into 0.3 mm quartz capillaries. Data were collected in the 2θ range 3–83° in two frames shifted by 0.5° in order to cover the 0.2° gaps between the modular detector elements every 5°. High temperature data were collected using a hot air blower (300–1248 K) and low temperature data were collected using a cyrostream (90–300 K).

Variable temperature neutron powder diffraction patterns for the samples $Sr_{1-x}Ti_{1-2x}Nb_{2x}O_3$ (x=0.15, 0.175, 0.2), were obtained using the ECHIDNA high resolution powder diffractometer at the OPAL reactor, Australian Nuclear Science and Technology Organisation [11]. All samples were placed into 9.5 mm vanadium cans. Diffraction patterns were obtained at room temperature and then a cryofurnace was used to obtain diffraction patterns of $Sr_{0.8}Ti_{0.6}Nb_{0.4}O_3$ at 75 and 4.2 K. Data were collected using a wavelength of 1.622 Å from 5° to 165° (2θ angle) with a step size of 0.05° over a period of 3.5 h for room temperature samples and 9.5 h for measurements performed at 75 and 4.2 K. Structural refinement was performed on both synchrotron X-ray and neutron powder diffraction data using the Rietveld method implemented in the software package Jana2006 [12]. The pseudo-Voigt profile shape function was assumed and the background was refined using a Chebyshev polynomial with nine terms.

Electron diffraction data were collected for the $Sr_{0.8}Ti_{0.6}Nb_{0.4}O_3$ phase. Specimens were prepared by crushing the powdered sample under ethanol and dispersing onto holey, carbon coated copper grids. These grids were then examined in a Philips EM430 transmission electron microscope operating at 300 kV. Single grains in different orientations were focused on and electron diffraction measurements performed.

3. Results and discussion

Over the composition range examined, there were three distinct regions with different species present. At low niobium content ($0 < x \le 0.125$), a $Sr_{1-x}Ti_{1-2x}Nb_{2x}O_3$ solid solution formed with minor $SrTiO_3$ intergrowth. $SrTiO_3$ appears to form rapidly in the early stages of STN synthesis. Additional heating and re-grinding was required to remove all traces of $SrTiO_3$. It was particularly difficult to remove for samples with $0 < x \le 0.125$, where the slow diffusion of small amounts of niobium meant that $SrTiO_3$ persisted as an impurity even on extended heating. The formation of $SrTiO_3$ intergrowth has been reported previously for related compounds by Pasero and Tilley [13], but not for the STN series. Similar to their observations the proportion of $SrTiO_3$ impurity present in our samples increased as the $SrTiO_3$ end member was approached. The effect of this intergrowth is evident in Fig. 1. The cell dimensions for $SrTiO_3$ [14] and the intergrowth free compositions fall on a straight line, while the observed cell dimensions for the samples that contain a small amount of intergrowth ($0 < x \le 0.125$) are slightly larger. This is consistent with their having a slightly higher niobium content. The unit cell parameters are therefore expected to be larger due to the larger ionic radius of niobium compared to titanium. The presence of $SrTiO_3$ has not been reported by Irvine et al. [6] or Kolodiazhnyi and Petric [7] for low niobium content despite similar synthesis methods being used. It is important to note, however, that the cell dimensions published by Irvine et al. [6] are slightly larger than our values for all compositions, consistent with $SrTiO_3$ intergrowth.

Using laboratory X-ray powder diffraction data the $SrTiO_3$ phase went undetected at first because its main reflections were overlapping with the Cu$K\alpha_2$ reflection from STN. Additionally, the Cu$K\alpha_2$ reflection of $SrTiO_3$ was only observed at higher angles where the two reflections ($K\alpha_1$ and $K\alpha_2$) were better resolved. This is in contrast to the synchrotron X-ray powder diffraction

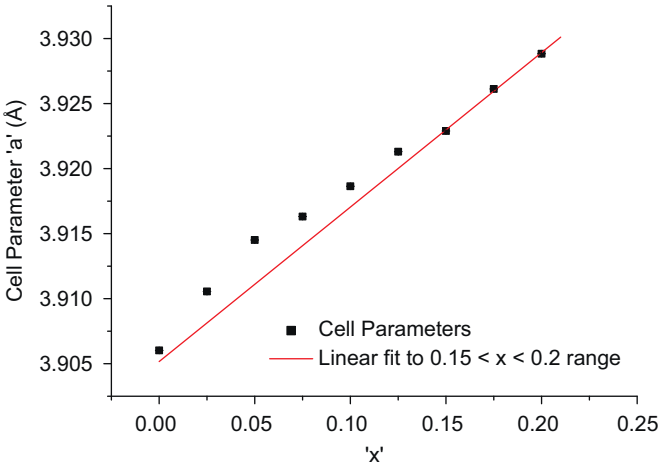

Fig. 1. Cell parameter variation across the $Sr_{1-x}Ti_{1-2x}Nb_{2x}O_3$ series as a function of parameter x. The deviation from linearity is highlighted by fitting a straight line to the pure solid solution range. Error bars are smaller than the data points.

data shown in Fig. 2 where $SrTiO_3$ is clearly resolved as an impurity phase at higher angles. The presence of $SrTiO_3$ should not be neglected as it had a clear and measurable impact on the exact composition of the STN sample.

$Sr_{1-x}Ti_{1-2x}Nb_{2x}O_3$ formed as a single-phase within the narrow composition range $0.15 \leq x \leq 0.2$. For the $0.2 < x < 0.4$ region, two distinct phases, $Sr_3TiNb_4O_{15}$ ($x=0.4$) and $Sr_{0.8}Ti_{0.6}Nb_{0.4}O_3$ ($x=0.2$) were identified, which is consistent with the results reported by Irvine et al. [6].

Synchrotron XRPD patterns were collected for all compositions synthesised in the region $0 \leq x \leq 0.2$. The lack of superlattice reflections in the diffraction patterns (see Fig. 3) suggests that the structure of the STN series is identical to that of the parent compound $SrTiO_3$, that is, an ideal cubic perovskite. Thus, as shown in Table 1, the best fit and most stable refinement obtained for all of the structures in the $Sr_{1-x}Ti_{1-2x}Nb_{2x}O_3$ ($0 \leq x \leq 0.2$) series applied the space group symmetry $Pm\bar{3}m$.

The substitution of Ti(IV) with Nb(V) should not cause significant disruption to the structure due to very similar bond

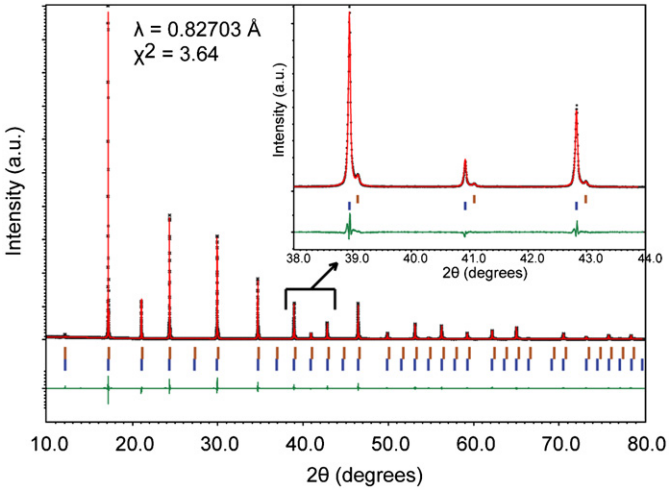

Fig. 2. The observed, calculated and difference synchrotron XRPD profiles of $Sr_{0.925}Ti_{0.85}Nb_{0.15}O_3$ collected at $\lambda=0.82703$ Å. The lower peak markers are of the main phase whereas the higher peak markers are of SrTiO3 impurity. The inset shows a region of the pattern where the $SrTiO_3$ reflections were clearly visible.

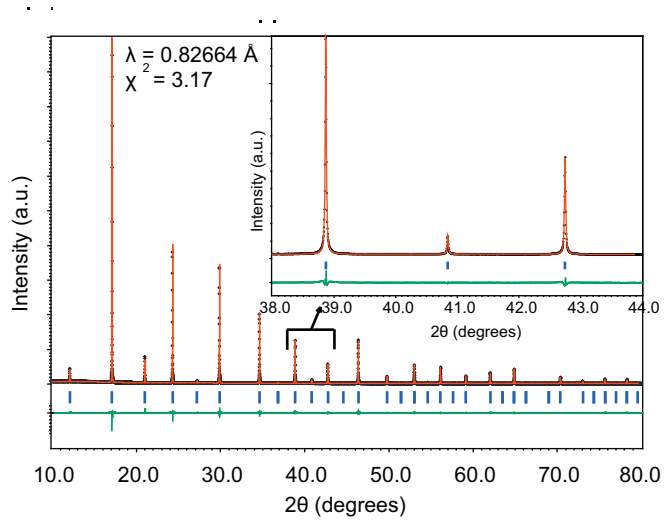

Fig. 3. The observed, calculated and difference synchrotron XRPD profiles for $Sr_{0.8}Ti_{0.6}Nb_{0.4}O_3$ collected at $\lambda=0.82664$ Å.

Table 1
Refined lattice parameters, space group, positional parameters and Debye–Waller factors for $Sr_{0.8}Ti_{0.6}Nb_{0.4}O_3$ collected at ambient conditions.

RT, $Pm\bar{3}m$, a=3.928831(1) Å, R_p—2.43, R_{wp}—3.22					
Atom	Site	x	y	z	B (Å^2)
Sr	1*b*	0.5	0.5	0.5	0.2150(5)
Ti	1*a*	0	0	0	0.2445(5)
Nb	1*a*	0	0	0	0.2445(5)
O	3*d*	0.5	0	0	0.271(5)

lengths to oxygen in an ideal undistorted octahedron. However, the structural effect of generating vacancies has not yet been fully discussed. The generation of a vacancy leads to the surrounding oxygen anions becoming partially under-bonded. In this circumstance, the oxygen anions shift slightly closer to adjacent strontium cations to maintain their bonding requirements. If the BO_6 octahedra are treated as rigid units, this shift must occur in the form of octahedral tilting. Evidence for such distortions was not observed in synchrotron X-ray diffraction patterns and so electron diffraction measurements were performed for $Sr_{0.8}Ti_{0.6}Nb_{0.4}O_3$.

Fig. 4 shows typical (a) $\langle 01\bar{4} \rangle$, (b) $\langle 11\bar{4} \rangle$ and (c) $\langle 13\bar{4} \rangle$ zone axis electron diffraction patterns (EDPs) that were obtained for $Sr_{0.8}Ti_{0.6}Nb_{0.4}O_3$. Note the presence of a complex but quite characteristic structured diffuse intensity distribution, which, to zeroth order, takes the form of $\mathbf{G} \pm \{0\,0\,1\}^*$ sheets of diffuse intensity. At different zone axis orientations, this diffuse distribution gives rise to relatively sharp diffuse streaking running through the parent perovskite Bragg reflections, **G**, perpendicular to one or other of the three $\langle 001 \rangle$ directions of real space in each of (A), (B) and (C), e.g. along $0\,4\,1^*$ in (A) and (B), along $4\,0\,1^*$ in (B) and (C) and along $0\,4\,3^*$ in (C). The continued presence of diffuse streaking of this type despite the changing incident beam orientation demonstrates that the streaking is not localised to that particular reciprocal space direction, but rather forms part of essentially continuous $\{001\}^*$ sheets of diffuse intensity in reciprocal space perpendicular to each of the $\langle 001 \rangle$ directions of real space.

This type of diffuse intensity distribution has previously been reported for $BaTiO_3$ and related compounds [15,16]. By analogy to $BaTiO_3$, the sheets of diffuse intensity can be explained by 1D-columnar displacements of the *B*-site cations and oxygen anions (as shown in Fig. 4D). That is, displacements or ordering of titanium or niobium along columns of octahedra, which do not correlate between adjacent chains of octahedra. It is proposed that the observed *B*-cation displacements are the result of second order Jahn–Teller effects, given that both Ti^{4+} and Nb^{5+} are d^0 transition metals [17]. Second order Jahn–Teller distortion occurs when the empty *d*-orbitals on the transition metals are low enough in energy to mix with the filled *p*-orbitals of the surrounding oxygen anions. In extended crystalline structures this results in nearly degenerate orbitals. The degeneracy can be removed through the spontaneous distortion of the d^0 cation away from the centre of the octahedron, lowering the energy of the crystal. Both Ti^{4+} and Nb^{5+} have been shown to preferentially distort toward the corners or edges of the octahedra, with Nb^{5+} experiencing stronger distortion than Ti^{4+} due to its higher electronegativity (lower energy orbitals) [18].

In addition to diffuse intensity there are some very minor features marked with arrows in Fig. 4A and B. These may be caused by increased octahedral rotations occurring on a local scale. That is, lattice vibrations may cause a greater deviation of the rigid octahedral units away from the zero tilt position on

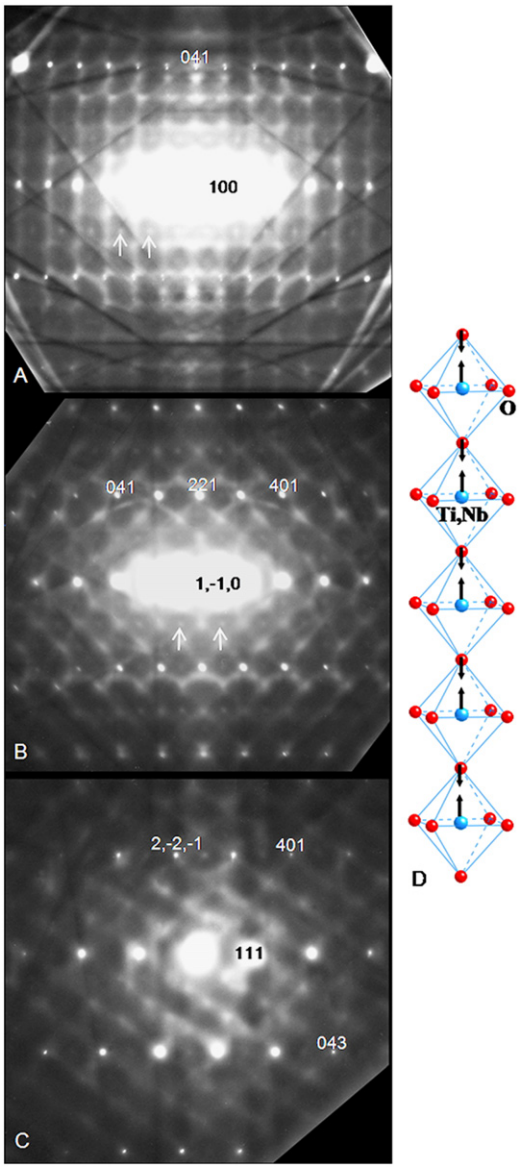

Fig. 4. EDPs of the A: ⟨01$\bar{4}$⟩, B: ⟨11$\bar{4}$⟩ and C: ⟨13$\bar{4}$⟩ zone axes of $Sr_{0.8}Ti_{0.6}Nb_{0.4}O_3$ displaying diffuse intensity present as sheets perpendicular to each of the three crystallographic axes. Weak superlattice reflections indicated with arrows. D: *B*-cation displacement within an one dimensional chain of octahedra.

Table 2
Linear thermal expansion co-efficient of $Sr_{0.8}Ti_{0.6}Nb_{0.4}O_3$ compared to $SrTiO_3$.

Composition	Temperature range (K)	α (K^{-1})
$Sr_{0.8}Ti_{0.6}Nb_{0.4}O_3$	90–1248	$8.72(9)\times10^{-6}$
$SrTiO_3$	300–2000	$3.23(2)\times10^{-5}$

average. Increased rotations due to enhanced structural flexibility have the additional effect of reducing the increase in unit cell parameters on heating. That is, for an ideal cubic perovskite the Ti/Nb–O–Ti/Nb bond angle is 180°. If the structure is slightly distorted however, this angle begins to deviate away from 180°. As the structure is heated then an increase in the lattice vibrations will lead to a greater deviation from 180° on average. As the angle deviates further from 180°, the distance between adjacent *B*-site cations will decrease, reducing the expansion of the unit cell.

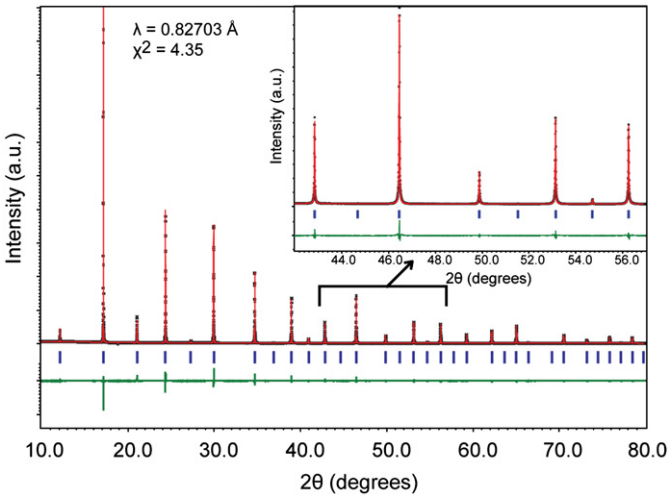

Fig. 5. The observed, calculated and difference synchrotron XRPD profiles for $Sr_{0.8}Ti_{0.6}Nb_{0.4}O_3$ at 90 K. Inset shows region where superlattice reflections were expected to appear at low temperature.

Table 2 shows a comparison of the thermal expansion parameter for $Sr_{0.8}Ti_{0.6}Nb_{0.4}O_3$ and $SrTiO_3$ [19]. Over a similar temperature range the rate of unit cell increase is less for $Sr_{0.8}Ti_{0.6}Nb_{0.4}O_3$ than it is in $SrTiO_3$. This suggests that the octahedral rotations are more prominent in $Sr_{0.8}Ti_{0.6}Nb_{0.4}O_3$ than the parent compound $SrTiO_3$.

Despite the similarities in the structure of $Sr_{0.8}Ti_{0.6}Nb_{0.4}O_3$ and $SrTiO_3$, $Sr_{0.8}Ti_{0.6}Nb_{0.4}O_3$ remains cubic down to 90 K as determined from synchrotron XRPD data (Fig. 5). This is in contrast to $SrTiO_3$, which undergoes a phase transition to tetragonal symmetry (space group *I*4/*mcm*) at 105 K [20–22]. Given the deviations in composition from the 'ideal cubic perovskite' $SrTiO_3$ this is an unexpected result. It is possible that the superlattice reflections resulting from small deviations in oxygen position were not present due to the weak X-ray scattering power of oxygen compared to strontium, niobium and titanium. Thus, in order to further explore the presence of octahedral distortions in $Sr_{0.8}Ti_{0.6}Nb_{0.4}O_3$ neutron powder diffraction data were collected at 75 K and at 4.2 K.

In both patterns there was no evidence of symmetry lowering in the form of peak splitting. However, Fig. 6 highlights a region at higher angles where weak R-point superlattice reflections resulting from out of phase tilting started to emerge around 75 K. As the superlattice reflections were barely visible in the 75 K pattern, Rietveld analysis was carried out on the pattern collected at 4.2 K. The structure was refined using the space group *I*4/*mcm* corresponding to an anti-phase tilt about the *c*-axis (tilt system $a^0a^0c^-$ in Glazer notation) [23]. The results of the refinement are provided in Table 3. A graphical representation of the distorted structure viewed along the *c*-axis is presented in Fig. 7. The transformation to tetragonal symmetry is analogous to the transition which occurs for $SrTiO_3$ at 105 K. It was expected that the transition in each structure would be similar, however it is surprising that the magnitude of octahedral tiling in $Sr_{0.8}Ti_{0.6}Nb_{0.4}O_3$ (1.404(1)°) is smaller at 4.2 K than what it is for $SrTiO_3$ (1.892(2)°). This indicates that, despite the presence of vacancies, the average structure of $Sr_{0.8}Ti_{0.6}Nb_{0.4}O_3$ is more stable in its cubic form than $SrTiO_3$.

4. Conclusion

In conclusion, the defect perovskite series $Sr_{1-x}Ti_{1-2x}Nb_{2x}O_3$ was investigated to determine its solid solution range and

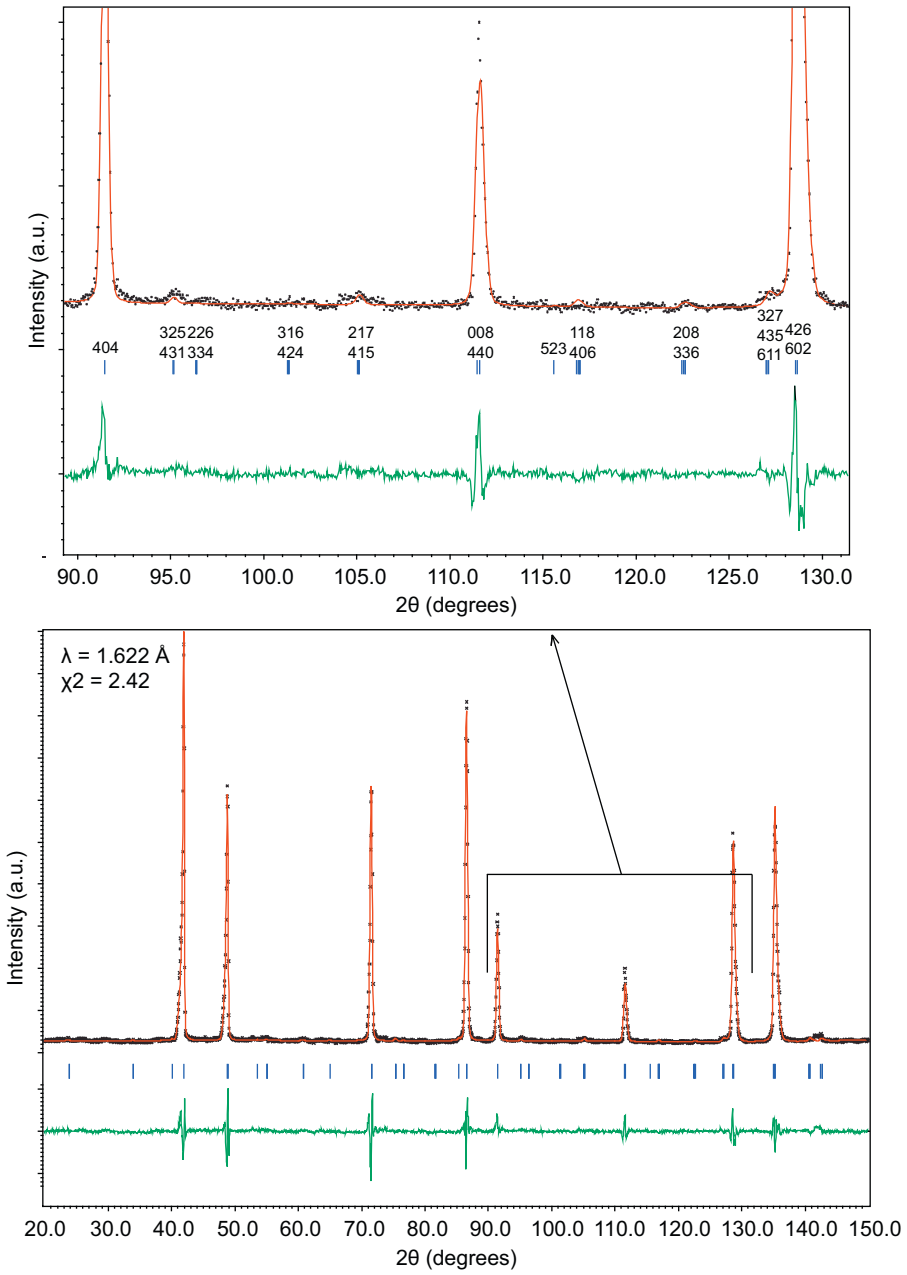

Fig. 6. The observed, calculated and difference neutron diffraction profiles for $Sr_{0.8}Ti_{0.6}Nb_{0.4}O_3$ at 4.2 K collected at 1.622 Å. The inset shows several diagnostic reflections — 325, 217 and 327/611 indicating doubling of the cell due to out of phase octahedral tilting.

Table 3
Refined lattice parameters, space group, positional parameters and Debye–Waller factors for $Sr_{0.8}Ti_{0.6}Nb_{0.4}O_3$ collected at 4.2 K.

T=4.2 K, $I4/mcm$, a=5.54663(8, c=7.8520(2) Å, R_p—6.92, R_{wp}—8.98					
Atom	Site	x	y	z	B (Å^2)
Sr	4*b*	0.5	0	0.25	0.27(4)
Ti	4*c*	0	0	0	0.5(1)
Nb	4*c*	0	0	0	0.5(1)
O1	4*a*	0	0	0.25	0.10(5)
O2	8*h*	0.2561(2)	0.7561(2)	0	0.14(2)

structural characteristics in order to synthesise a phase with the highest *A*-site vacancy concentration and with the ideal cubic structure. Three separate regions were observed: $0 < x \leq 0.125$ was a solid solution of $Sr_{1-x}Ti_{1-2x}Nb_{2x}O_3$ with some minor $SrTiO_3$ intergrowth, $0.125 < x \leq 0.2$ was a pure $Sr_{1-x}Ti_{1-2x}Nb_{2x}O_3$ solid solution and for $0.2 < x < 0.4$ two phases formed, i.e. $Sr_{0.8}Ti_{0.6}Nb_{0.4}O_3$ and $Sr_3TiNb_4O_{15}$. The end member with the highest concentration of vacancies, $Sr_{0.8}Ti_{0.6}Nb_{0.4}O_3$, exhibited a cubic structure over the temperature range 90–1248 K with a thermal expansion co-efficient $8.72(9) \times 10^{-6}$ K^{-1} for this region. The apparent lack of distortion upon extensive niobium substitution and over a wide temperature range was proposed to be due to local distortions of the *B*-site d^0 cations along one dimensional chains and octahedral rotations which allow additional degrees of flexibility in the structure. The cubic perovskite structure was retained down to a temperature of ~75 K below which anti-phase octahedral tilting about the *c*-crystallographic axis lowered the symmetry to tetragonal. This transition is analogous to that occurring in $SrTiO_3$ at 105 K; however, it is more difficult to detect due to extremely weak nature of the distortions. The observed flexibility of this

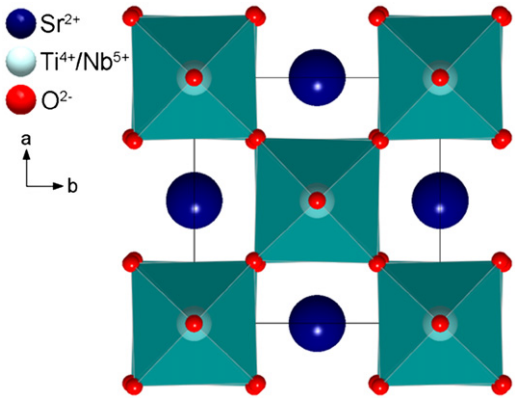

Fig. 7. Representation of the low temperature tetragonal unit cell for $Sr_{0.8}Ti_{0.6}Nb_{0.4}O_3$ projected along the *c*-axis highlighting the anti-phase tilting which 'locks-in' below 75 K.

defect perovskite leading to structural stability over a very wide range of temperatures will make it a good candidate for applications where such stability is required. For the purposes of lithium intercalation, e.g., it is desirable that very little structural change occurs on insertion and removal of lithium from the structure. Thus, the observed structural flexibility of STN would make it an ideal candidate for reversible lithium intercalation and this will be further investigated.

Acknowledgments

Collection of synchrotron X-ray diffraction data at the Australian Synchrotron was supported by the Australian Synchrotron Research Program, which is funded by the Commonwealth of Australia under the Access to Major Research Facilities Program. Neutron powder data collection at the OPAL reactor was supported by the Australian Institute of Nuclear Science and Engineering (AINSE award ALNBRG00974N).

References

[1] V.M. Goldschmidt, Naturwissenschaften 14 (1926) 477.
[2] P.M. Woodward, Acta Crystallogr. B53 (1997) 32.
[3] T. Ohzuku, R.J. Brodd, J. Power Sources 174 (2007) 449.
[4] M.S. Whittingham, Chem. Rev. 104 (2004) 4271.
[5] T.-Y. Tien, C.J. Moratis, J. Am. Ceram. Soc. 50 (1967) 392.
[6] J.T.S. Irvine, P.R. Slater, P.A. Wright, Ionics 2 (1996) 213.
[7] T. Kolodiazhnyi, A. Petric, J. Electroceram. 15 (2005) 5.
[8] B. Hessen, S.A. Sunshine, T. Siegrist, R. Jimenez, Mater. Res. Bull. 26 (1991) 85.
[9] I.D. Brown, D. Altermatt, Acta Crystallogr. B41 (1985) 244.
[10] B. Schmitt, C. Brönnimann, E.F. Eikenberry, F. Gozzo, C. Hörmann, R. Horisberger, B. Patterson, Nucl. Instrum. Methods A 501 (2003) 267.
[11] K.-D. Liss, B.A. Hunter, M.E. Hagen, T.J. Noakes, S.J. Kennedy, Physica B 385-386 (2006) 1010.
[12] V. Petříček, M. Dušek, L. Palatinus, Jana2006. The crystallographic computing system. Institute of Physics, Praha, Czech Republic, 2006.
[13] D. Pasero, R.J.D. Tilley, J. Solid State Chem. 135 (1998) 260.
[14] T. Mitsui, S. Nomura (Eds.), Landolt-Börnstein: Numerical Data and Functional Relationships in Science and Technology, vol. 16, Springer-Verlag, Berlin, 1982.
[15] Y. Liu, R.L. Withers, B. Nguyen, K. Elliott, Appl. Phys. Lett. 91 (2007) 152907.
[16] Y. Liu, R.L. Withers, X. Wei, J.D. Fitz Gerald, J. Solid State Chem. 180 (2007) 858.
[17] N.S.P. Bhuvanesh, J. Gopalakrishnan, J. Mater. Chem. 7 (1997) 2297.
[18] P.S. Halasyamani, Chem. Mater. 16 (2004) 3586.
[19] D. de Ligny, P. Richet, Phys. Rev. B: Condens. Matter 53 (1996) 3013.
[20] R.A. Cowley, Philos. Trans. R. Soc. A 354 (1996) 2799.
[21] A. Okazaki, M. Kawaminami, Mater. Res. Bull. 8 (1973) 545.
[22] H. Unoki, T. Sakudo, J. Phys. Soc. Jpn. 23 (1967) 546.
[23] A.M. Glazer, Acta Crystallogr. 28 (1972) 3384.